HGWaveNet: A Hyperbolic Graph Neural Network for Temporal Link Prediction

Qijie Bai
College of CS, TJ Key Lab of NDST
Nankai University
Tianjin, China
qijie.bai@mail.nankai.edu.cn

Changli Nie
College of CS, TJ Key Lab of NDST
Nankai University
Tianjin, China
nie_cl@mail.nankai.edu.cn

Haiwei Zhang*
College of CS, TJ Key Lab of NDST
Nankai University
Tianjin, China
zhhaiwei@nankai.edu.cn

Dongming Zhao
China Mobile Communication Group
Tianjin Co., Ltd
Tianjin, China
waitman_840602@163.com

Xiaojie Yuan
College of CS, TJ Key Lab of NDST
Nankai University
Tianjin, China
yuanxj@nankai.edu.cn

ABSTRACT

Temporal link prediction, aiming to predict future edges between paired nodes in a dynamic graph, is of vital importance in diverse applications. However, existing methods are mainly built upon uniform Euclidean space, which has been found to be conflict with the power-law distributions of real-world graphs and unable to represent the hierarchical connections between nodes effectively. With respect to the special data characteristic, hyperbolic geometry offers an ideal alternative due to its exponential expansion property. In this paper, we propose HGWaveNet, a novel hyperbolic graph neural network that fully exploits the fitness between hyperbolic spaces and data distributions for temporal link prediction. Specifically, we design two key modules to learn the spatial topological structures and temporal evolutionary information separately. On the one hand, a hyperbolic diffusion graph convolution (HDGC) module effectively aggregates information from a wider range of neighbors. On the other hand, the internal order of causal correlation between historical states is captured by hyperbolic dilated causal convolution (HDCC) modules. The whole model is built upon the hyperbolic spaces to preserve the hierarchical structural information in the entire data flow. To prove the superiority of HGWaveNet, extensive experiments are conducted on six real-world graph datasets and the results show a relative improvement by up to 6.67% on AUC for temporal link prediction over SOTA methods.

CCS CONCEPTS

• **Theory of computation → Dynamic graph algorithms**; • **Computing methodologies → Dimensionality reduction and manifold learning**; **Neural networks**.

---

*Corresponding author.

KEYWORDS

Temporal link prediction, hyperbolic geometry, graph neural network, diffusion graph convolution, dilated causal convolution

1 INTRODUCTION

Dynamic graphs, derived from the general graphs by adding an additional temporal dimension, have attracted a lot of attention in recent years [14]. It has become a general practice to abstract real-world complex systems (e.g. traffic systems [58], social networks [50] and e-commerce platforms [16]) to this newly data structure due to its powerful ability for modeling the temporal interactions between entities. Temporal link prediction, aiming to forecast future relationships between nodes, is of vital importance for understanding the evolution of dynamic graphs [49].

According to the expression of temporal information, dynamic graphs can be divided into two categories: continuous dynamic graphs and discrete dynamic graphs [54]. Continuous dynamic graphs, also called graph streams, can be viewed as groups of edges ordered by time and each edge is associated with a timestamp. Recording topological structures of a dynamic graph at constant time intervals as snapshots, the list of snapshots is defined as a discrete dynamic graph. In comparison, continuous dynamic graphs keep all temporal information [17], but discrete dynamic graphs are more computationally efficient benefiting from the coarse-grained updating frequency [24]. This paper studies temporal link prediction on discrete dynamic graphs.

Existing studies have put forward some approaches to dynamic graph embedding and temporal link prediction. Most of them focus on two main contents: the **spatial topological structure** and the **temporal evolutionary information** of dynamic graphs. For instance, CTDNE [25] runs temporal random walks to capture both spatial and temporal information on graphs. TDGNN [30] introduces a temporal aggregator for GNNs to aggregate historical information of neighbor nodes and edges. Hawkes process [15, 60]
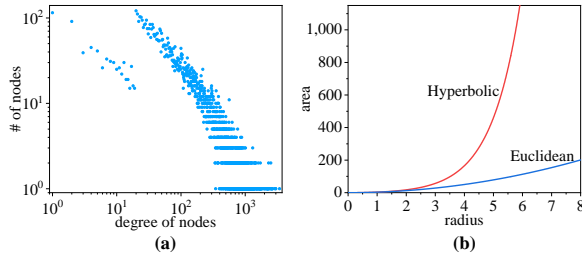
Figure 1: (a) The degree distribution of real-world network MovieLens. Coordinate axes are logarithmic. (b) Areas of circles on hyperbolic spaces (curvature $c = -1$) and Euclidean spaces, which shows that the hyperbolic spaces expand exponentially while Euclidean spaces expand polynomially.

is also applied to simulate the evolution of graphs. Furthermore, DyRep [40] leverages recurrent neural networks to update node representations over time. TGAT [7] uses the multi-head attention mechanism [42] and a sampling strategy that fixes the number of neighbor nodes involved in message-propagation to learn both spatial and temporal information.

These methods are all built upon Euclidean spaces. However, recent works [3, 19] have noticed that most real-world graph data, such as social networks, always exhibit implicit hierarchical structures and power-law distributions (as shown in Figure 1(a)) rather than uniform grid structures which fit Euclidean spaces best. The mismatches between data distributions and space geometries severely limit the performances of Euclidean models [4, 26].

Hyperbolic spaces are those of constant negative curvatures, and are found to keep great representation capacity for data with hierarchical structures and power-law distributions due to the exponential expansion property (as shown in Figure 1(b)) [19, 29]. In the past few years, researchers have made some progress in representing hierarchical data in hyperbolic spaces [4, 22, 26, 27, 33, 44, 52, 56]. HTGN [52] attempts to embed dynamic graphs into hyperbolic geometry and achieves state-of-the-art performance. It adopts hyperbolic GCNs to capture spatial features and a hyperbolic temporal contextual attention module to extract the historical information. However, this method faces two major shortcomings. First, for some large graphs with long paths, the message propagation mechanism of GCNs is not effective enough because only direct neighbor nodes can be calculated in each step. Second, the temporal contextual attention module cannot handle the internal order of causal correlation in historical data and thus loses valid information for temporal evolutionary process.

To address the two aforementioned shortcomings of HTGN, in this paper, we propose a novel hyperbolic graph neural network model named HGWaveNet for temporal link prediction. In HGWaveNet, we first project the nodes into hyperbolic spaces. Then in the aspect of spatial topology, a hyperbolic diffusion graph convolution (HDGC) module is designed to learn node representations of each snapshot effectively from both direct neighbors and indirectly connected nodes. For temporal information, recurrent neural networks always emphasize short time memory while ignoring that of long time due to the time monotonic assumption [6], and the attention mechanism ignores the causal orders in temporality. Inspired

by WaveNet [41] and Graph WaveNet [48], we present hyperbolic dilated causal convolution (HDCC) modules to obtain hidden cumulative states of nodes by aggregating historical information and capturing temporal dependencies. In the training process of each snapshot, the hidden cumulative states and spatial-based node representations are fed into a hyperbolic gated recurrent unit (HGRU). The outputs of HGRU are regarded as the integration of spatial topological structures and temporal evolutionary information, and are utilized for final temporal link prediction. A hyperbolic temporal consistency (HTC) [52] component is also leveraged to ensure stability for tracking the evolution of graphs.

To conclude, the main contributions of this paper are as follows:

- We propose a novel hyperbolic graph neural network model named HGWaveNet for temporal link prediction, which learns both spatial hierarchical structures and temporal causal correlation of dynamic graphs.
- With regard to spatial topological structures, we design a hyperbolic diffusion graph convolution (HDGC) module to fit the power-law distributions of data and aggregate information from a wider range of nodes with greater effectiveness.
- For temporal evolution, we present hyperbolic dilated causal convolution (HDCC) modules to capture the internal causality between snapshots, and a hyperbolic temporal consistency (HTC) component is applied to remain stable when learning the evolution of graphs.
- We conduct extensive experiments on diverse real-world dynamic graphs. The results prove the superiority of HGWaveNet, as it has a relative improvement by up to 6.67% in terms of AUC over state-of-the-art methods.

2 RELATED WORK

In this section, we systematically review the relevant works on temporal link prediction and hyperbolic graph representation learning.

2.1 Temporal Link Prediction

Temporal link prediction on dynamic graphs has attracted increasing interests in the past few years. Early methods usually use traditional algorithms or shallow neural architectures to represent structural and temporal information. For instance, CTDNE [25] captures the spatial and temporal information simultaneously by adding temporal constraints to random walk. Another example of using temporal random walk is DynNode2vec [23], which updates the sampled sequences incrementally at each snapshot rather than generating them anew. DynamicTriad [59] imposes the triad closure process and models the evolution of graphs by developing closed triads from open triads. Furthermore, Change2vec [2] improves this process and makes it applicable for dynamic heterogeneous graphs. HTNE [60] integrates the Hawkes process into graph embedding to learn the influence of historical neighbors on current neighbors.

In contrast, graph neural network methods have recently received increasing attention. GCN [46] provides an excellent node embedding pattern for general tasks on graphs, and most of later models take GCN or its variants, such as GraphSAGE [12] and GAT [43], as basic modules for learning topological structures. GCRN [36] feeds node representations learned from GCNs into a modified LSTM to obtain the temporal information. Similar ideas are

explored in EvolveGCN [28], E-LSTM-D [5] and NTF [47]. The main difference between EvolveGCN and E-LSTM-D is that EvolveGCN could be considered as a combination of GCN and RNN while E-LSTM-D uses LSTM together with an encoder-decoder architecture. NTF takes a reverse order that characterizes the temporal interactions with LSTM before adopting the MLP for non-linearities between different latent factors, and sufficiently learns the evolving characteristics of graphs. To better blend the spatial and temporal node features, DySAT [34] proposes applying multi-head self-attention. TGN [31] leverages memory modules with GCN operators and significantly increases the computational efficiency. TNS [45] provides an adaptive receptive neighborhood for each node at any time. VRGNN [11] models the uncertainty of node embeddings by regarding each node in each snapshot as a distribution.

However, the prevailing methods are built upon Euclidean spaces, which are not isometric with the power-law distributions of real-world graphs, and may cause distortion with the graph scale grows.

2.2 Hyperbolic Graph Representation Learning

Representation learning in hyperbolic spaces has been noticed due to their fitness to the hierarchical structures of real-world data. The significant performance advantages shown by the shallow Poincaré [26] and Lorentz [27] models spark more attempts to this issue. Integrated with graph neural networks, HGNN [22] and HGCN [4] are designed for graph classification and node embedding tasks separately. HAT [56] exploits attention mechanism for hyperbolic node information propagation and aggregation. LGCN [57] builds the graph operations of hyperbolic GCNs with Lorentzian version and rigorously guarantees that the learned node features follow the hyperbolic geometry. The above hyperbolic GNN-based models all adopt the bi-directional transition between a hyperbolic space and corresponding tangent spaces, while a tangent space is the first-order approximation of the original space and may inevitably cause distortion. To avoid distortion, H2H-GCN [8] develops a manifold-preserving graph convolution and directly works on hyperbolic manifolds. For practical application situations, HGCF [37], HRCF [53] and HICF [51] study the hyperbolic collaborative filtering for user-item recommendation systems. Through hyperbolic graph learning, HyperStockGAT [35] captures the scale-free spatial and temporal dependencies in stock prices, and achieves state-of-the-art stock forecasting performance.

HVGNN [38] and HTGN [52] fill the gap of hyperbolic models on dynamic graphs. HVGNN generates stochastic node representations of hyperbolic normal distributions via a hyperbolic graph variational autoencoder to represent the uncertainty of dynamics. HTGN adopts a conventional model architecture that handles the spatial and temporal information with HGCNs and contextual attention modules separately, however, ignores the causal order in the graph evolution. To further improve the hyperbolic graph models especially on temporal link prediction problem, we propose our HGWaveNet in terms of discrete dynamic graphs.

3 PRELIMINARIES

In this section, we first give the formalized definitions of discrete dynamic graphs and temporal link prediction. Then some critical fundamentals about hyperbolic geometry are introduced.
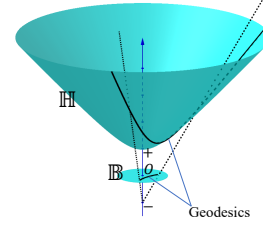

Figure 2: A hyperbolic manifold $\mathbb{H}$ and the corresponding Poincaré ball model $\mathbb{B}$. The distances on the manifolds are measured along geodesics.

3.1 Problem Definition

This paper discusses temporal link prediction on discrete dynamic graphs. Following [18], we define discrete dynamic graphs as:

*Definition 3.1 (**Discrete Dynamic Graphs**). In discrete dynamic graph modeling, dynamic graphs can be viewed as a sequence of snapshots sampled from the original evolving process at consecutive time points. Formally, discrete dynamic graphs are represented as $\mathcal{G} = (\mathcal{G}_0, \mathcal{G}_1, \cdots, \mathcal{G}_T)$, in which $\mathcal{G}_t$ is a snapshot at timestamp t. The time granularity for snapshot divisions could be hours, days, months or even years depending on specific datasets and applications.*

Based on Definition 3.1, temporal link prediction is described as:

*Definition 3.2 (**Temporal Link Prediction**). The aim of temporal link prediction is to predict the links appeared in the snapshots after timestamp t based on the observed snapshots before timestamp t. Formally, the model takes $(\mathcal{G}_0, \mathcal{G}_1, \cdots, \mathcal{G}_{t-1})$ as input in the training process, and then makes predictions on $(\mathcal{G}_t, \mathcal{G}_{t+1}, \cdots, \mathcal{G}_T)$.*

3.2 Hyperbolic Geometry of the Poincaré Ball

The n-dimensional hyperbolic space $(\mathbb{H}^n_c, g^{c,\mathbb{H}})$ is the unique simply connected n-dimensional complete Riemannian manifold $\mathbb{H}^n_c$ with a constant negative curvature $-c(c > 0)$, and $g^{c,\mathbb{H}}$ is the Riemannian metric. The tangent space $\mathcal{T}_{\mathbf{x}}\mathbb{H}^n_c$ is a Euclidean, local, first-order approximation of $\mathbb{H}^n_c$ around the point $\mathbf{x} \in \mathbb{H}^n_c$. Similar to [26] and [9], we construct our method based on the Poincaré ball, one of the most widely used isometric models of hyperbolic spaces. Corresponding to $(\mathbb{H}^n_c, g^{c,\mathbb{H}})$, the Poincaré ball $(\mathbb{B}^n_c, g^{c,\mathbb{B}})$ is defined as

$$\mathbb{B}^n_c := \left\{ \mathbf{x} \in \mathbb{R}^n : c\|\mathbf{x}\|^2 < 1 \right\},$$
$$g^{c,\mathbb{B}}_{\mathbf{x}} := \left(\lambda^c_{\mathbf{x}} \right)^2 g^E, \quad \lambda^c_{\mathbf{x}} := \frac{2}{1 - c\|\mathbf{x}\|^2}, \tag{1}$$

where $g^E = \mathbf{I}_n$ is the Euclidean metric tensor.

The Poincaré ball manifold $\mathbb{B}^n_c$ is an open ball of radius $1/\sqrt{c}$ (see Figure 2). The induced distance between two points $\mathbf{x}, \mathbf{y} \in \mathbb{B}^n_c$ is measured along a geodesic and given by[1]

$$d_c(\mathbf{x}, \mathbf{y}) = \frac{2}{\sqrt{c}} \cdot \tanh^{-1}\left(\sqrt{c}\| - \mathbf{x} \oplus_c \mathbf{y}\| \right), \tag{2}$$

in which the Möbius addition $\oplus_c$ in $\mathbb{B}^n_c$ is defined as

$$\mathbf{x} \oplus_c \mathbf{y} := \frac{\left(1 + 2c\langle\mathbf{x}, \mathbf{y}\rangle + c\|\mathbf{y}\|^2\right)\mathbf{x} + \left(1 - c\|\mathbf{x}\|^2\right)\mathbf{y}}{1 + 2c\langle\mathbf{x}, \mathbf{y}\rangle + c^2\|\mathbf{x}\|^2\|\mathbf{y}\|^2}. \tag{3}$$

---

[1]$-\mathbf{x} \oplus_c \mathbf{y}$ should be read as $(-\mathbf{x}) \oplus_c \mathbf{y}$ rather than $-(\mathbf{x} \oplus_c \mathbf{y})$.

To map points between hyperbolic spaces and tangent spaces, exponential and logarithmic maps are given [9]. For $\mathbf{x}, \mathbf{y} \in \mathbb{B}_c^n, \mathbf{v} \in \mathcal{T}_{\mathbf{x}} \mathbb{B}_c^n, \mathbf{x} \neq \mathbf{y}$ and $\mathbf{v} \neq \mathbf{0}$, the exponential map $\exp_{\mathbf{x}}^c : \mathcal{T}_{\mathbf{x}} \mathbb{B}_c^n \to \mathbb{B}_c^n$ is

$$\exp_{\mathbf{x}}^c(\mathbf{v}) = \mathbf{x} \oplus_c \left(\tanh \left(\frac{\sqrt{c} \lambda_{\mathbf{x}}^c \|\mathbf{v}\|}{2} \right) \frac{\mathbf{v}}{\sqrt{c} \|\mathbf{v}\|} \right), \tag{4}$$

and the logarithmic map $\log_{\mathbf{x}}^c : \mathbb{B}_c^n \to \mathcal{T}_{\mathbf{x}} \mathbb{B}_c^n$ is

$$\log_{\mathbf{x}}^c(\mathbf{y}) = d_c(\mathbf{x}, \mathbf{y}) \frac{-\mathbf{x} \oplus_c \mathbf{y}}{\lambda_{\mathbf{x}}^c \| - \mathbf{x} \oplus_c \mathbf{y} \|}, \tag{5}$$

where $\lambda_{\mathbf{x}}^c$ and $d_c(\mathbf{x}, \mathbf{y})$ are the same as in Equations (1) and (2). In our method, we use the origin point $\mathbf{o}$ as the reference point $\mathbf{x}$ to balance the errors in diverse directions.

4 METHODOLOGY

This section describes our proposed model HGWaveNet. First, we elaborate on the details of two core components: hyperbolic diffusion graph convolution (HDGC) and hyperbolic dilated causal convolution (HDCC). Then other key modules contributing to HGWaveNet are introduced, including gated HDCC, hyperbolic gated recurrent unit (HGRU), hyperbolic temporal consistency (HTC) and Fermi-Dirac decoder. Finally, we summarize the overall framework of HGWaveNet and analyse the time complexity.

4.1 Hyperbolic Diffusion Graph Convolution

Hyperbolic graph convolutional neural networks (HGCNs [4]) are built analogous to traditional GNNs. A typical HGCN layer consists of three key parts: hyperbolic feature transform

$$\mathbf{h}_i^{l,\mathbb{B}} = \mathbf{W}^l \otimes_{c^{l-1}} \mathbf{x}_i^{l-1,\mathbb{B}} \oplus_{c^{l-1}} \mathbf{b}^l, \tag{6}$$

attention-based neighbor aggregation

$$\begin{aligned} \mathbf{y}_i^{l,\mathbb{B}} &= \mathrm{Agg}_{c^l}(\mathbf{h}^{l,\mathbb{B}})_i \\ &= \exp_{\mathbf{o}}^{c^l} \left(\mathrm{Att} \left(\mathrm{Concat}_{j \in \mathcal{N}(i)} \left(\log_{\mathbf{o}}^{c^{l-1}} \left(\mathbf{h}_j^{l,\mathbb{B}} \right) \right) \right) \right), \end{aligned} \tag{7}$$

and hyperbolic activation

$$\mathbf{x}_i^{l,\mathbb{B}} = \exp_{\mathbf{o}}^{c^l} \left(\sigma \left(\log_{\mathbf{o}}^{c^l} \left(\mathbf{y}_i^{l,\mathbb{B}} \right) \right) \right), \tag{8}$$

in which $\mathbf{W}^l, \mathbf{b}^l$ are trainable parameters and $\mathbf{x}_i^{l,\mathbb{B}}$ is the representation of node i at layer l in manifold $\mathbb{B}_{c^l}^n$. Following [52], the matrix-vector multiplication $\otimes_c$ is defined as

$$\mathbf{M} \otimes_c \mathbf{x} := \exp_{\mathbf{o}}^c \left(\mathbf{M} \log_{\mathbf{o}}^c(\mathbf{x}) \right), \quad \mathbf{M} \in \mathbb{R}^{n \times n}, \mathbf{x} \in \mathbb{B}_c^n. \tag{9}$$

However, the shallow HGCN can only aggregate information of direct neighbors and is not effective enough for large graphs with long paths. To overcome this shortcoming, we impose the diffusion process referring to [21]. Consider a random walk process with restart probability α on $\mathcal{G}$, and a state transition matrix $\mathbf{P}$ (for most situations, $\mathbf{P}$ is the normalized adjacent matrix). Such Markov process converges to a stationary distribution $\mathcal{P} \in \mathbb{R}^{n \times n}$ after many steps, the i-th row of which is the likelihood of diffusion from node i. The stationary distribution $\mathcal{P}$ can be calculated in the closed form [39]

$$\mathcal{P} = \sum_{k=0}^{\infty} \alpha(1-\alpha)^k \mathbf{P}^k, \tag{10}$$

where k is the diffusion step. In practice, a finite K-step truncation of the diffusion process is adopted and separate trainable weight
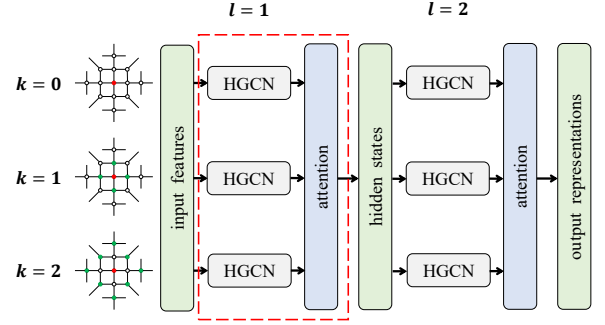

Figure 3: A hyperbolic diffusion graph convolution (HDGC) module with the number of layers $L = 2$ and the number of diffusion steps $K = 2$. The part in red dashed rectangle is a complete HDGC layer.

matrices are added to each step for specific objective tasks. Then, the diffusion convolution layer on graphs is defined as

$$\mathbf{Z} = \sum_{k=0}^{K} \mathbf{A}^k \mathbf{X} \mathbf{W}_k, \tag{11}$$

in which $\mathbf{A}$ is the bi-direct adjacent matrix, $\mathbf{X}$ is the input node features, $\mathbf{W}_k$ is the weight matrix for the k-th diffusion step, and $\mathbf{Z}$ is the output node representations.

On account of the sparsity of real-world data, we convert the graph convolution into equivalent spatial domains for efficiency. Do all above operations in the hyperbolic space, and replace the summation in Equation (11) with an attention mechanism for better information aggregation. Then, the k-th step of hyperbolic diffusion graph convolution at layer l is

$$\mathbf{X}_k^l = \mathrm{HGCN}_{c_k^l} \left(\mathbf{A}^k, \mathbf{X}^{l-1} \right), \tag{12}$$

where $\mathrm{HGCN}_{c^l}(\cdot)$ is the conjunctive form of Equations (6), (7), and (8) with the adjacent matrix and node features as inputs. $\mathbf{X}^l$ is calculated as

$$\mathbf{X}^l = \exp_{\mathbf{o}}^{c^l} \left(\mathrm{Att} \left(\mathrm{Concat}_k \left(\log_{\mathbf{o}}^{c_k^l} \left(\mathbf{X}_k^l \right) \right) \right) \right). \tag{13}$$

Hyperbolic diffusion graph convolution is finally constructed with the stack of layers defined by Equations (13) and (12), as sketched in Figure 3.

4.2 Hyperbolic Dilated Causal Convolution

Causal convolution refers to applying a convolution filter only to data at past timestamps [41], and guarantees that the order of data modeling is not violated, which means that the prediction $p(x_t|x_0, x_1, \cdots, x_{t-1})$ emitted by the model at timestamp t cannot depend on future data $x_t, x_{t+1}, \cdots, x_T$. For 1-D temporal information, this operation can be implemented by shifting the output of a normal convolution with kernel size S by $\lfloor S/2 \rfloor$ steps, but a sufficiently large receptive field requires stacking many layers. To decrease the computational cost, dilated convolutions are adopted. By skipping the inputs with a certain step d, a dilated convolution applies its kernel over a larger area than its length, and with the
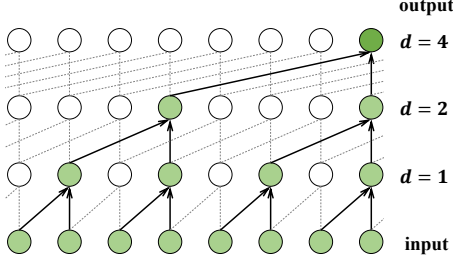
Figure 4: A stacked hyperbolic dilated causal convolution (HDCC) module with dilated depth $D = 3$ and kernel size $S = 2$. Each circle refers to one node at a timestamp. Under the exponentially large receptive field, each node preserves the temporal causal correlations with the past S^D snapshots.

stack of dilated convolution layers, the receptive field expands exponentially while preserving high computational efficiency. Based on the above definitions of causal convolutions and dilated convolutions, the dilated causal convolution operation in manifold $\mathbb{B}_c^n$ can be formalized mathematically as

$$(\mathbf{Z}_i \odot \mathbf{F})_t = \exp_{\mathbf{o}}^c \left(\sum_{s=0}^{S-1} \mathbf{F}_s \log_{\mathbf{o}}^c \left(\mathbf{Z}_{i,t-d \times s} \right) \right), \qquad (14)$$

where d is the dilation step, $\mathbf{Z}_{i,t} \in \mathbb{B}_c^n$ ($t \leq T$) is the representation of node i at snapshot $\mathcal{G}_t$ and $\mathbf{F} \in \mathbb{R}^{S \times n}$ denotes the kernels for all dimensions (also called channels). A stacked hyperbolic dilated causal convolution module is shown in Figure 4.

Compared to attention-based historical information aggregation [52], HDCC can learn the internal order of causal correlation in temporality. Meanwhile, compared to RNNs, HDCC allows parallel computation and alleviates vanishing or exploding gradient problems due to its non-recursion[48]. Considering the superiority of HDCC on sequence problems, we leverage this module in handling the temporal evolutionary information of graphs.

4.3 Other Key Modules in HGWaveNet

Except for HDGC and HDCC, some other modules contribute greatly to our proposed HGWaveNet. Based on HDCC, we further design gated HDCC to preserve the valid historical information. Hyperbolic gated recurrent unit (HGRU) [52] is able to efficiently learn the latest node representations in Poincaré ball from historical states and current spatial characteristics. Additionally, as defined in [52], hyperbolic temporal consistency (HTC) module provides a similarity constraint in temporality to ensure stability during graph evolution. Finally, a Fermi-Dirac decoder [19] is used to compute the probability scores for edge reconstruction.

4.3.1 Gated HDCC. As shown in the left part of Figure 5, we adopt a simple gating mechanism on the outputs of HDCCs. What is noteworthy is the use of logarithmic map before the Euclidean activation functions and exponential map after gating. The formulation is described as

$$\mathbf{H}_{i,t} = \exp_{\mathbf{o}}^c \left(\tanh \left(\log_{\mathbf{o}}^c \left((\mathbf{Z}_i \odot \mathbf{F}_1)_t \right) \right) \cdot \sigma \left(\log_{\mathbf{o}}^c \left((\mathbf{Z}_i \odot \mathbf{F}_2)_t \right) \right) \right),$$
$$(15)$$

where $\mathbf{F}_1$ and $\mathbf{F}_2$ are different convolution kernels for two HDCCs, $\mathbf{H}_{i,t} \in \mathbb{B}_c^n$ ($t \leq T$) is the historical hidden state of node i at snapshot $\mathcal{G}_t$, and $\cdot$ denotes element-wise product. In addition, to enable a deeper model for learning more implicit information, residual and skip connections are applied throughout the gated HDCC layers.

4.3.2 Hyperbolic Gated Recurrent Unit. HGRU [52] is the hyperbolic variant of GRU [6]. Performed in the tangent space, HGRU computes the output with high efficiency from historical hidden states and current input features, as

$$\mathbf{Z}_{i,t} = \exp_{\mathbf{o}}^c \left(\mathrm{GRU} \left(\log_{\mathbf{o}}^c \left(\mathbf{X}_{i,t} \right), \log_{\mathbf{o}}^c \left(\mathbf{H}_{i,t-1} \right) \right) \right). \qquad (16)$$

In HGWaveNet, the historical hidden states are from gated HDCC module, so we use a single HGRU cell for just one step rather than linking it into recursion.

4.3.3 Hyperbolic Temporal Consistency. In real-world graphs, the evolution proceeds continuously. Correspondingly, the node representations are expected to change gradually in terms of temporality, which means that the node representations at two consecutive snapshots should keep a short distance. Hence, HTC [52] defines a similarity constraint penalty between $\mathbf{Z}_{t-1}$ and $\mathbf{Z}_t$ at snapshot $\mathcal{G}_t$ as

$$\mathcal{L}_{\mathrm{HTC}}^t = \frac{1}{N} \sum_{i=1}^{N} d_c \left(\mathbf{Z}_{i,t-1}, \mathbf{Z}_{i,t} \right), \qquad (17)$$

where $d_c(\cdot)$ is defined in Equation (2) and N is the number of nodes. By adding the penalty in optimization process, HTC ensures that the node representations do not change rapidly and the stability of graph evolution is achieved.

4.3.4 Fermi-Dirac Decoder. As a generalization of sigmoid, Fermi-Dirac decoder [19] gives a probability score for edges between nodes i and j, which fits the temporal link prediction problem greatly. It is defined as

$$p_{F-D} \left(\mathbf{x}_i, \mathbf{x}_j \right) = \frac{1}{\exp \left(\left(d_c \left(\mathbf{x}_i, \mathbf{x}_j \right) - r \right) / s \right) + 1}, \qquad (18)$$

where r and s are hyper-parameters, and $\mathbf{x}_i, \mathbf{x}_j \in \mathbb{B}_c^n$ are hyperbolic representations of nodes i and j.

4.4 Framework of HGWaveNet

With all modules introduced above, we now summarize the overall framework of HGWaveNet in Figure 5. For the snapshot $\mathcal{G}_{t-1} \in \mathcal{G}$, we first project the input node features into the hyperbolic space with exponential map, and then an HDGC module is applied to learn the spatial topological structure characteristics denoted by $\mathbf{X}_{t-1}$. Simultaneously, the stacked gated HDCC layers calculate the latest historical hidden state $\mathbf{H}_{t-2}$ from previous node representations $\mathbf{Z}_{t-2}, \mathbf{Z}_{t-3}, \cdots$ (the initial historical node representations are padded randomly at the beginning of training). Next, the spatial information $\mathbf{X}_{t-1}$ and the temporal information $\mathbf{H}_{t-2}$ are inputted into a single HGRU cell. The output of HGRU $\mathbf{Z}_{t-1}$ is exactly the new latest node representations at snapshot $\mathcal{G}_{t-1}$, and is fed into the Fermi-Dirac decoder to make temporal link predictions for snapshot $\mathcal{G}_t$.

To maximize the probability of connected nodes in $\mathcal{G}_t$ and minimize the probability of unconnected nodes, we use a cross-entropy
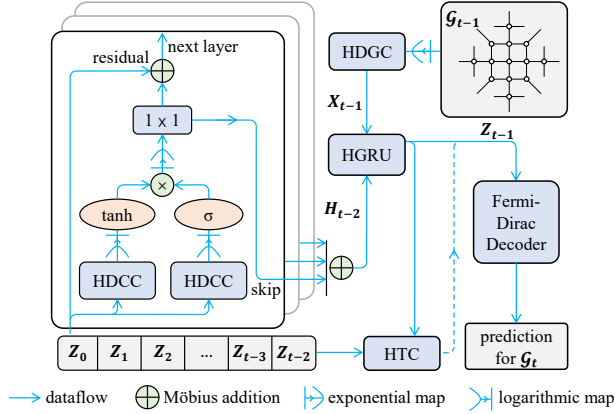
Figure 5: The overall framework of HGWaveNet. For $\mathcal{G}_{t-1}$, the historical evolutionary information handled by gated HDCCs and the spatial topological information handled by HDGC are fed into an HGRU module. With the constraint of HTC, the hyperbolic outputs are decoded by a Fermi-Dirac decoder and the temporal link prediction for $\mathcal{G}_t$ is made.

like loss $\mathcal{L}_{CE}^t$ defined as

$$
\begin{aligned}
\mathcal{L}_{CE}^t = &\text{Avg}_{i\sim_t j}\left(-\log\left(p_{F-D}\left(\mathbf{Z}_{i,t-1}, \mathbf{Z}_{j,t-1}\right)\right)\right) + \\
&\text{Avg}_{i'\nsim_t j'}\left(-\log\left(1 - p_{F-D}\left(\mathbf{Z}_{i',t-1}, \mathbf{Z}_{j',t-1}\right)\right)\right),
\end{aligned}
\tag{19}
$$

in which $\sim_t$ denotes the connection at snapshot $\mathcal{G}_t$ between two nodes, and $\nsim_t$ is the opposite. (i', j') is the sampled negative edge for accelerating training and preventing over-smoothing. Taking the HTC module into account and summing up all snapshots, the complete loss function is

$$
\mathcal{L} = \sum_{t=0}^{T}\left(\mathcal{L}_{CE}^t + \lambda\mathcal{L}_{HTC}^t\right).
\tag{20}
$$

Time Complexity Analysis. We analyse the time complexity of our proposed HGWaveNet by module for each snapshot. For the HDGC module, the computation is of $O((Nd^2 + |\mathcal{E}_t|Kd)L)$, where d is the dimension of node representations, $|\mathcal{E}_t|$ is the edge number for snapshot $\mathcal{G}_t$, K is the truncated diffusion steps and L is the layer number of HDGC. For gated HDCC, the time complexity is $O(S^D dD')$, in which S and D are the kernel size and dilated depth of a single HDCC, respectively, and D' is the layer number of the complete gated HDCC module. HGRU and HTC run only once for each snapshot, and both take the time complexity of $O(Nd)$. For Fermi-Dirac decoder, the time complexity is $O(|\mathcal{E}_t|d + |\tilde{\mathcal{E}}_t|d)$, in which $|\tilde{\mathcal{E}}_t|$ is the number of negative samples for snapshot $\mathcal{G}_t$.

5 EXPERIMENTS AND ANALYSIS

In this section, we conduct extensive experiments on six real-world graphs and prove the superiority of our proposed HGWaveNet. In addition, we also conduct ablation studies and hyper-parameter analysis to corroborate the three primary ideas of our method: the fitness between graph distributions and hyperbolic geometry, the effectiveness of spatial information from a wider range of neighbors

Table 1: Statistics of datasets.

Datasets	Enron	DBLP	AS733	FB	HepPh	MovieLens
# Nodes	184	315	6,628	45,435	15,330	9,746
# Edges	790	943	13,512	180,011	976,097	997,837
# Snapshots	11	10	30	36	36	11
Train : Test	8:3	7:3	20:10	33:3	30:6	8:3
δ	1.5	2.0	1.5	2.0	1.0	2.0

Table 2: Baselines.

Methods	Static/dynamic	Manifolds
HGCN [4]	Static	Lorentz
HAT[56]	Static	Poincaré
EvolveGCN [28]	Dynamic	Euclidean
GRUGCN [36]	Dynamic	Euclidean
TGN [31]	Dynamic	Euclidean
DySAT [34]	Dynamic	Euclidean
HTGN [52]	Dynamic	Poincaré

aggregated by HDGC, and the causality of historical information in the evolutionary process learned by HDCC.

5.1 Experimental Setup

5.1.1 Datasets. We evaluate our proposed model and baselines on six real-world datasets from diverse areas, including email communication networks Enron[2] [1], academic co-author networks DBLP[3] [11] and HepPh[4] [20], Internet router networks AS733[5] [20], social networks FB[6] [32] and movie networks MovieLens[7] [13]. The statistics of these datasets are shown in Table 1. We take the same splitting ratios for training and testing as [52] on all datasets except MovieLens on which a similar manner is adopted. Gromov's hyperbolicity [10] δ is used to measure the tree-likeness and hierarchical properties of graphs. A lower δ denotes a more tree-like structure and $\delta = 0$ denotes a pure tree. The datasets we choose all remain implicitly hierarchical and show distinct power-law distributions.

5.1.2 Baselines. Considering that HGWaveNet is constructed in the hyperbolic space for dynamic graphs, we choose seven competing baselines either in hyperbolic spaces or built for dynamic graphs to verify the superiority of our model. The baselines are summarized in Table 2, where HTGN on Poincaré ball shows state-of-the-art performance in most evaluations.

5.1.3 Evaluation Tasks and Metrics. Similar to [52], our experiments consist of two different tasks: *temporal link prediction* and *temporal new link prediction*. Specifically, *temporal link prediction* aims to predict the edges that appear in $\mathcal{G}_t$ and other snapshots after timestamp t based on the training on $(\mathcal{G}_0, \mathcal{G}_1, \cdots, \mathcal{G}_{t-1})$, while *temporal new link prediction* aims to predict those in $\mathcal{G}_t$ but not in $\mathcal{G}_{t-1}$. To quantify the experimental performance, we choose the widely used metrics average precision (AP) and area under ROC curve (AUC). The datasets are split into training sets and test sets as shown in Table 1 by snapshots to run both our proposed model and baselines on the above tasks.

---

[2]https://www.cs.cornell.edu/~arb/data/email-Enron/
[3]https://github.com/VGraphRNN/VGRNN/tree/master/data
[4]https://snap.stanford.edu/data/cit-HepPh.html
[5]https://snap.stanford.edu/data/as-733.html
[6]https://networkrepository.com/ia-facebook-wall-wosn-dir.php
[7]https://grouplens.org/datasets/movielens/

Table 3: Performance on temporal link prediction.

	Dataset	Enron		DBLP		AS733		FB		HepPh		MovieLens	
	Metric	AUC	AP	AUC	AP	AUC	AP	AUC	AP	AUC	AP	AUC	AP
Baselines	HGCN	93.96 ± 0.09	93.55 ± 0.06	89.16 ± 0.16	91.63 ± 0.22	96.34 ± 0.05	93.28 ± 0.11	<u>86.11 ± 0.13</u>	83.74 ± 0.15	90.64 ± 0.07	88.98 ± 0.09	84.89 ± 0.40	77.98 ± 0.66
	HAT	<u>94.49 ± 0.11</u>	<u>94.63 ± 0.08</u>	<u>89.29 ± 0.18</u>	90.15 ± 0.14	96.09 ± 0.01	93.21 ± 0.02	84.02 ± 0.09	83.03 ± 0.15	90.52 ± 0.04	<u>89.53 ± 0.04</u>	86.26 ± 0.14	84.19 ± 0.21
	EvolveGCN	90.12 ± 0.69	92.71 ± 0.34	83.88 ± 0.53	87.53 ± 0.22	92.47 ± 0.04	95.28 ± 0.01	76.85 ± 0.85	80.87 ± 0.64	76.82 ± 1.46	81.18 ± 0.89	55.41 ± 1.55	69.41 ± 1.00
	GRUGCN	92.47 ± 0.36	93.38 ± 0.24	84.60 ± 0.92	87.87 ± 0.58	94.96 ± 0.35	96.64 ± 0.22	79.38 ± 1.02	82.77 ± 0.75	82.86 ± 0.53	85.87 ± 0.23	71.01 ± 0.77	79.04 ± 0.53
	TGN	91.77 ± 1.04	85.36 ± 0.87	87.20 ± 0.82	84.87 ± 0.80	93.19 ± 1.03	92.27 ± 0.83	80.85 ± 0.23	81.92 ± 1.34	74.78 ± 0.47	74.61 ± 0.43	71.52 ± 0.59	70.53 ± 0.38
	DySAT	93.06 ± 0.97	93.06 ± 1.05	87.25 ± 1.70	90.40 ± 1.47	95.06 ± 0.21	96.72 ± 0.12	76.88 ± 0.08	80.39 ± 0.14	81.02 ± 0.25	84.47 ± 0.23	70.21 ± 0.58	78.41 ± 0.33
	HTGN	94.17 ± 0.17	94.31 ± 0.26	89.26 ± 0.17	<u>91.91 ± 0.07</u>	<u>98.75 ± 0.03</u>	<u>98.41 ± 0.03</u>	83.70 ± 0.33	<u>83.80 ± 0.43</u>	<u>91.13 ± 0.14</u>	89.52 ± 0.28	<u>86.80 ± 0.34</u>	<u>85.40 ± 0.19</u>
Ours	HGWaveNet	**96.86 ± 0.08**	**97.04 ± 0.07**	**89.96 ± 0.27**	**92.12 ± 0.18**	**98.78 ± 0.01**	**98.53 ± 0.02**	**89.51 ± 0.28**	**86.88 ± 0.29**	**92.37 ± 0.04**	**91.48 ± 0.05**	**91.90 ± 0.06**	**90.65 ± 0.12**
	Gain(%)	+2.51	+2.55	+0.75	+0.23	+0.03	+0.12	+3.95	+3.68	+1.36	+2.18	+5.88	+6.15
Ablation	w/o HDGC	94.95 ± 0.10	95.24 ± 0.07	89.51 ± 0.24	91.84 ± 0.17	97.97 ± 0.20	97.35 ± 0.24	85.99 ± 0.29	82.77 ± 0.48	90.61 ± 0.22	89.68 ± 0.03	84.35 ± 0.12	82.77 ± 0.38
	Gain(%)	-1.97	-1.85	-0.50	-0.30	-0.82	-1.20	-3.93	-4.73	-1.91	-1.97	-8.22	-8.69
	w/o HDCC	95.33 ± 0.09	95.64 ± 0.09	89.56 ± 0.22	92.04 ± 0.12	97.83 ± 0.17	97.25 ± 0.21	85.13 ± 0.16	82.38 ± 0.88	90.83 ± 0.20	89.77 ± 0.32	82.46 ± 0.37	80.29 ± 0.58
	Gain(%)	-1.58	-1.44	-0.44	-0.09	-0.96	-1.30	-4.89	-5.18	-1.67	-1.87	-10.27	-11.43
	w/o 𝔹	92.62 ± 0.55	93.77 ± 0.33	85.18 ± 0.29	87.76 ± 0.11	95.21 ± 0.11	96.85 ± 0.08	79.20 ± 0.34	82.45 ± 0.21	76.31 ± 0.75	78.11 ± 0.29	73.70 ± 0.54	80.15 ± 0.54
	Gain(%)	-4.38	-3.37	-5.31	-4.73	-3.61	-1.71	-11.52	-5.10	-17.39	-14.62	-19.80	-11.58

* For evaluations on baselines and our model, the best results are in bold, and the suboptimal results are underlined. The same applies to Table 4.

★ Part of results are from [52] under the same experimental setup. The same applies to Table 4.

Table 4: Performance on temporal new link prediction.

	Dataset	Enron		DBLP		AS733		FB		HepPh		MovieLens	
	Metric	AUC	AP	AUC	AP	AUC	AP	AUC	AP	AUC	AP	AUC	AP
Baselines	HGCN	90.36 ± 0.16	88.33 ± 0.55	81.20 ± 0.19	83.28 ± 0.23	92.33 ± 0.12	88.31 ± 0.16	81.04 ± 0.14	80.59 ± 0.13	89.64 ± 0.27	87.87 ± 0.11	85.27 ± 0.35	78.56 ± 0.49
	HAT	90.34 ± 0.10	88.60 ± 0.19	79.29 ± 0.15	82.58 ± 0.08	91.65 ± 0.08	90.13 ± 0.15	<u>83.05 ± 0.10</u>	<u>82.96 ± 0.18</u>	89.63 ± 0.05	<u>88.34 ± 0.04</u>	86.54 ± 0.16	84.60 ± 0.25
	EvolveGCN	82.85 ± 0.97	85.01 ± 0.22	73.49 ± 0.86	77.11 ± 0.44	75.82 ± 0.67	83.57 ± 0.46	74.49 ± 0.89	78.33 ± 0.66	74.79 ± 1.61	79.04 ± 1.02	55.45 ± 1.53	69.35 ± 0.98
	GRUGCN	87.59 ± 0.57	88.41 ± 0.45	75.60 ± 1.60	78.55 ± 1.05	83.14 ± 1.21	88.14 ± 0.76	77.69 ± 1.03	81.07 ± 0.77	81.97 ± 0.49	84.78 ± 0.22	71.32 ± 0.77	79.51 ± 0.50
	TGN	86.75 ± 0.59	81.37 ± 0.42	<u>81.83 ± 1.08</u>	81.61 ± 0.62	87.89 ± 0.63	84.94 ± 0.94	78.93 ± 0.98	76.57 ± 0.63	74.21 ± 0.78	76.12 ± 0.54	72.22 ± 0.68	70.90 ± 0.40
	DySAT	87.94 ± 3.78	86.83 ± 5.01	79.74 ± 4.35	83.47 ± 3.01	82.84 ± 0.72	89.07 ± 0.57	74.97 ± 0.12	78.34 ± 0.07	79.01 ± 0.26	82.53 ± 0.25	70.63 ± 0.58	79.02 ± 0.33
	HTGN	<u>91.26 ± 0.27</u>	<u>90.62 ± 0.34</u>	81.74 ± 0.56	<u>84.06 ± 0.41</u>	<u>96.62 ± 0.22</u>	<u>95.52 ± 0.25</u>	82.21 ± 0.41	81.70 ± 0.46	<u>90.11 ± 0.14</u>	88.18 ± 0.31	<u>87.06 ± 0.25</u>	<u>85.82 ± 0.29</u>
Ours	HGWaveNet	**93.49 ± 0.08**	**92.51 ± 0.10**	**84.26 ± 0.46**	**86.19 ± 0.33**	**96.99 ± 0.07**	**95.60 ± 0.10**	**88.59 ± 0.24**	**86.00 ± 0.30**	**91.45 ± 0.05**	**90.21 ± 0.04**	**92.04 ± 0.04**	**90.66 ± 0.07**
	Gain(%)	+2.44	+2.09	+2.97	+2.53	+0.38	+0.08	+6.67	+3.66	+1.49	+2.12	+5.72	+5.64
Ablation	w/o HDGC	90.67 ± 0.20	89.90 ± 0.22	83.47 ± 0.36	85.85 ± 0.28	95.69 ± 0.34	93.99 ± 0.36	84.96 ± 0.30	81.57 ± 0.42	89.63 ± 0.26	88.27 ± 0.03	84.76 ± 0.15	83.42 ± 0.33
	Gain(%)	-3.02	-2.82	-0.94	-0.39	-1.34	-1.68	-4.10	-5.15	-1.99	-2.15	-7.91	-7.99
	w/o HDCC	91.76 ± 0.08	90.87 ± 0.06	82.36 ± 0.23	84.87 ± 0.10	94.56 ± 0.44	92.91 ± 0.45	84.03 ± 0.14	80.99 ± 0.76	89.87 ± 0.20	88.42 ± 0.30	82.92 ± 0.31	81.23 ± 0.50
	Gain(%)	-1.85	-1.77	-2.25	-1.53	-2.51	-2.81	-5.15	-5.83	-1.73	-1.98	-9.91	-10.40
	w/o 𝔹	87.10 ± 0.72	88.49 ± 0.57	76.65 ± 0.80	79.53 ± 0.67	84.85 ± 0.77	89.59 ± 0.37	77.37 ± 0.33	80.63 ± 0.19	74.23 ± 0.58	76.21 ± 0.53	74.11 ± 0.55	80.51 ± 0.31
	Gain(%)	-6.83	-4.35	-9.03	-7.73	-12.52	-6.29	-12.67	-6.24	-18.83	-15.52	-19.48	-11.20

5.2 Experimental Results

We implement HGWaveNet[8] with PyTorch on Ubuntu 18.04. Each experiment is repeated five times to avoid random errors, and the average results (with form *average value ± standard deviation*) on the test sets are reported in Table 3 and Table 4. Next, we discuss the experimental results on each evaluation task separately.

5.2.1 Temporal Link Prediction. The results on temporal link prediction are shown in Table 3. Obviously, our HGWaveNet outperforms all baselines including the hyperbolic state-of-the-art model HTGN both on AUC and AP. To analyse the results further, we intuitively divide the six datasets into two groups: small (Enron, DBLP, AS733) and large (FB, HepPh, MovieLens), according to the scales. It can be observed that the superiority of our model is more significant on large graphs than small ones compared with baselines, especially those Euclidean methods. This is because the representation capacity of Euclidean methods decreases rapidly with increasing graph scales, while hyperbolic models remain stable by virtue of the fitness between data distributions and space properties.

5.2.2 Temporal New Link Prediction. The results on temporal new link prediction are shown in Table 4. This task aims to predict the edges unseen in the training process and evaluates the inductive ability of models. Our model shows greater advantages, and similar gaps with those on temporal link prediction between small and large graphs appear again. Another observed fact is that even for the inductive evaluation task, the two hyperbolic static methods HGCN and HAT have a relatively better performance than the Euclidean dynamic models. This observation further demonstrates the excellence of modeling real-world graphs on hyperbolic spaces.

5.3 Ablation Study

To asses the contribution of each component, we conduct the following ablation study on three HGWaveNet variants:

- **w/o HDGC:** HGWaveNet without the hyperbolic diffusion graph convolution, implemented by replacing HDGC with shallow HGCN to learn from spatial characteristics.
- **w/o HDCC:** HGWaveNet without the hyperbolic dilated causal convolution, implemented by replacing HDCC with an attention mechanism to achieve historical hidden states.

---

[8]The code is open sourced in https://github.com/TaiLvYuanLiang/HGWaveNet.

- **w/o $\mathbb{B}$:** HGWaveNet without hyperbolic geometry, implemented by replacing all modules with corresponding Euclidean versions.

We take the same experimental setup with HGWaveNet and baselines on these three variants, and the results are reported in the last rows of Table 3 and Table 4. The performance drops noticeably after removing any of these three components, which indicates their respective importance. In the following, we discuss the details of the effectiveness of these variants.

HDGC module imposes the diffusion process into hyperbolic graph convolution networks. It allows nodes to aggregate information from a wider range of neighbors and improves the efficiency of message propagation by calculating the stationary distribution of a long Markov process in a closed form. The fact that performance of w/o HDGC variant has a larger degradation on large graphs than small ones forcefully proves the effectiveness of this component for large graphs with long paths.

The purpose of HDCC module is to capture the internal order of causal correlation in sequential data. Generally, the larger a graph is, the more complex its evolution is and the richer historical information it has. The experimental results on w/o HDCC show the powerful ability of this component to capture causal order in temporal evolution process, especially on complex graphs (i.e. FB and MovieLens).

As observed in Table 3 and Table 4, the degradation of w/o $\mathbb{B}$ is much more severe than that of the other two variants, which strongly supports our primary idea that hyperbolic geometry fits the power-law distributions of real-world graphs very well. Moreover, it is noteworthy that for most results, the variant w/o $\mathbb{B}$ exhibits a comparable or even exceeding performance to other Euclidean baselines. This proves that our model architecture still keeps advanced even without the advantages of hyperbolic geometry.

5.4 Parameter Analysis

We further study the influences of three hyper-parameters: representation dimension, truncated diffusion step and dilated depth.

We evaluate the performance of HGWaveNet and one of the best Euclidean models GRUGCN on two datasets FB (relatively sparse) and MovieLens (relatively dense) by setting the representation dimension into different values, as shown in Figure 6. On the one hand, it is clear that with the dimension decreasing, our model remains stable compared to GRUGCN, to which the hyperbolic geometry contributes greatly. On the other hand, for HGWaveNet, the degradation of the performance on MovieLens is severer than that on FB, which is consistent with the conclusion in [55] that hyperbolic models fit sparse data better than dense data.

Figure 7 shows the results of our model for temporal link prediction on MovieLens with different values of truncated diffusion step K in HDGC and dilated depth D in HDCC. The wrap-up observation that the performance generally increases as K and D increase proves the positive influences of diffusion process and dilation convolution. Specifically, in terms of truncated diffusion step, the performance has a great improvement from $K = 1$ to $K = 2$. When $K > 2$, the benefit from increasing K becomes too small to match the surge of computation from exponentially expanding neighbors in graphs. Dilated depth D is used to control the receptive field of
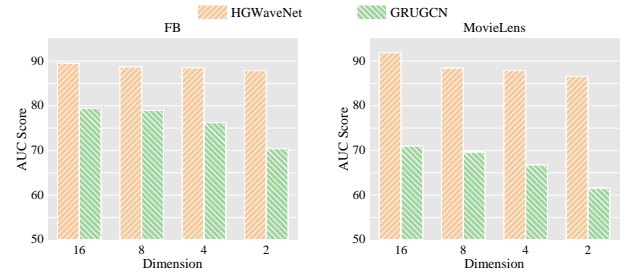

Figure 6: The influence of representation dimension on two datasets FB and MovieLens for HGWaveNet and GRUGCN.
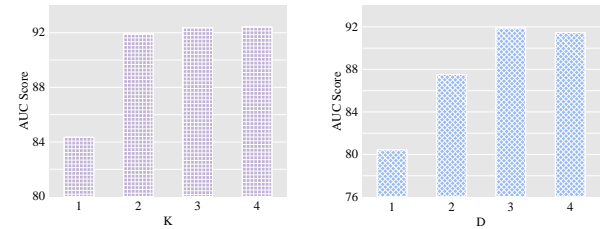

Figure 7: The influence of truncated diffusion step K (left) and dilated depth D (right) on MovieLens.

causal convolution. However, as the receptive field expands, more noise is imported and may degrade the model performance. According to our extensive experiments, $D = 3$ is a nice choice in most situations, with the causal convolution kernel size being 2.

6 CONCLUSION

In this paper, we propose a hyperbolic graph neural network HGWaveNet for temporal link prediction. Inspired by the observed power-law distribution and implicit hierarchical structure of real-world graphs, we construct our model on the Poincaré ball, one of the isometric models of hyperbolic spaces. Specifically, we design two novel modules hyperbolic diffusion graph convolution (HDGC) and hyperbolic dilated causal convolution (HDCC) to extract the spatial topological information and temporal evolutionary states, respectively. HDGC imposes the diffusion process into graph convolution and provides an efficient way to aggregate information from a wider range of neighbors. HDCC ensures that the internal order of causal correlations is not violated by applying the convolution filter only to previous data. Extensive experiments on diverse real-world datasets prove the superiority of HGWaveNet, and the ablation study further verifies the effectiveness of each component of our model. In future work, we will further generalize our model for more downstream tasks and try to use hyperbolic GNNs to capture more complex semantic information in heterogeneous graphs.

REFERENCES

[1] Austin R Benson, Rediet Abebe, Michael T Schaub, Ali Jadbabaie, and Jon Kleinberg. 2018. Simplicial closure and higher-order link prediction. *Proceedings of the National Academy of Sciences* 115, 48 (2018), E11221–E11230.

[2] Ranran Bian, Yun Sing Koh, Gillian Dobbie, and Anna Divoli. 2019. Network embedding and change modeling in dynamic heterogeneous networks. In *Proceedings of the 42nd International ACM SIGIR Conference on Research and Development in Information Retrieval.* 861–864.

[3] Michael M Bronstein, Joan Bruna, Yann LeCun, Arthur Szlam, and Pierre Vandergheynst. 2017. Geometric deep learning: going beyond euclidean data. *IEEE Signal Processing Magazine* 34, 4 (2017), 18–42.

[4] Ines Chami, Zhitao Ying, Christopher Ré, and Jure Leskovec. 2019. Hyperbolic graph convolutional neural networks. *Advances in neural information processing systems* 32 (2019).

[5] Jinyin Chen, Jian Zhang, Xuanheng Xu, Chenbo Fu, Dan Zhang, Qingpeng Zhang, and Qi Xuan. 2019. E-lstm-d: A deep learning framework for dynamic network link prediction. *IEEE Transactions on Systems, Man, and Cybernetics: Systems* 51, 6 (2019), 3699–3712.

[6] Kyunghyun Cho, Bart van Merrienboer, Çaglar Gülçehre, Dzmitry Bahdanau, Fethi Bougares, Holger Schwenk, and Yoshua Bengio. 2014. Learning Phrase Representations using RNN Encoder-Decoder for Statistical Machine Translation. In *EMNLP*.

[7] da Xu, chuanwei ruan, evren korpeoglu, sushant kumar, and kannan achan. 2020. Inductive representation learning on temporal graphs. In *International Conference on Learning Representations.* https://openreview.net/forum?id=rJeW1yHYwH

[8] Jindou Dai, Yuwei Wu, Zhi Gao, and Yunde Jia. 2021. A hyperbolic-to-hyperbolic graph convolutional network. In *Proceedings of the IEEE/CVF Conference on Computer Vision and Pattern Recognition.* 154–163.

[9] Octavian Ganea, Gary Bécigneul, and Thomas Hofmann. 2018. Hyperbolic neural networks. *Advances in neural information processing systems* 31 (2018).

[10] M GROMOV. 1987. Hyperbolic groups, Essays in group theory. *MSRI Publ.* 8 (1987), 75–264.

[11] Ehsan Hajiramezanali, Arman Hasanzadeh, Krishna Narayanan, Nick Duffield, Mingyuan Zhou, and Xiaoning Qian. 2019. Variational graph recurrent neural networks. *Advances in neural information processing systems* 32 (2019).

[12] Will Hamilton, Zhitao Ying, and Jure Leskovec. 2017. Inductive representation learning on large graphs. *Advances in neural information processing systems* 30 (2017).

[13] F Maxwell Harper and Joseph A Konstan. 2015. The movielens datasets: History and context. *Acm transactions on interactive intelligent systems (tiis)* 5, 4 (2015), 1–19.

[14] Petter Holme and Jari Saramäki. 2012. Temporal networks. *Physics reports* 519, 3 (2012), 97–125.

[15] Hong Huang, Ruize Shi, Wei Zhou, Xiao Wang, Hai Jin, and Xiaoming Fu. 2021. Temporal Heterogeneous Information Network Embedding.. In *IJCAI.* 1470–1476.

[16] Houye Ji, Junxiong Zhu, Xiao Wang, Chuan Shi, Bai Wang, Xiaoye Tan, Yanghua Li, and Shaojian He. 2021. Who you would like to share with? a study of share recommendation in social e-commerce. In *Proceedings of the AAAI Conference on Artificial Intelligence*, Vol. 35. 232–239.

[17] David Kempe, Jon Kleinberg, and Amit Kumar. 2000. Connectivity and inference problems for temporal networks. In *Proceedings of the thirty-second annual ACM symposium on Theory of computing.* 504–513.

[18] Shima Khoshraftar and Aijun An. 2022. A Survey on Graph Representation Learning Methods. *arXiv preprint arXiv:2204.01855* (2022).

[19] Dmitri Krioukov, Fragkiskos Papadopoulos, Maksim Kitsak, Amin Vahdat, and Marián Boguná. 2010. Hyperbolic geometry of complex networks. *Physical Review E* 82, 3 (2010), 036106.

[20] Jure Leskovec, Jon Kleinberg, and Christos Faloutsos. 2005. Graphs over time: densification laws, shrinking diameters and possible explanations. In *Proceedings of the eleventh ACM SIGKDD international conference on Knowledge discovery in data mining.* 177–187.

[21] Yaguang Li, Rose Yu, Cyrus Shahabi, and Yan Liu. 2018. Diffusion Convolutional Recurrent Neural Network: Data-Driven Traffic Forecasting. In *International Conference on Learning Representations.*

[22] Qi Liu, Maximilian Nickel, and Douwe Kiela. 2019. Hyperbolic graph neural networks. *Advances in Neural Information Processing Systems* 32 (2019).

[23] Sedigheh Mahdavi, Shima Khoshraftar, and Aijun An. 2018. dynnode2vec: Scalable dynamic network embedding. In *2018 IEEE international conference on big data (Big Data).* IEEE, 3762–3765.

[24] Naoki Masuda and Renaud Lambiotte. 2016. *A guide to temporal networks.* World Scientific.

[25] Giang Hoang Nguyen, John Boaz Lee, Ryan A Rossi, Nesreen K Ahmed, Eunyee Koh, and Sungchul Kim. 2018. Continuous-time dynamic network embeddings. In *Companion proceedings of the the web conference 2018.* 969–976.

[26] Maximillian Nickel and Douwe Kiela. 2017. Poincaré embeddings for learning hierarchical representations. *Advances in neural information processing systems* 30 (2017).

[27] Maximillian Nickel and Douwe Kiela. 2018. Learning continuous hierarchies in the lorentz model of hyperbolic geometry. In *International Conference on Machine Learning.* PMLR, 3779–3788.

[28] Aldo Pareja, Giacomo Domeniconi, Jie Chen, Tengfei Ma, Toyotaro Suzumura, Hiroki Kanezashi, Tim Kaler, Tao Schardl, and Charles Leiserson. 2020. Evolvegcn: Evolving graph convolutional networks for dynamic graphs. In *Proceedings of the AAAI Conference on Artificial Intelligence*, Vol. 34. 5363–5370.

[29] Wei Peng, Tuomas Varanka, Abdelrahman Mostafa, Henglin Shi, and Guoying Zhao. 2021. Hyperbolic Deep Neural Networks: A Survey. *IEEE Transactions on Pattern Analysis and Machine Intelligence* (2021).

[30] Liang Qu, Huaisheng Zhu, Qiqi Duan, and Yuhui Shi. 2020. Continuous-time link prediction via temporal dependent graph neural network. In *Proceedings of The Web Conference 2020.* 3026–3032.

[31] Emanuele Rossi, Ben Chamberlain, Fabrizio Frasca, Davide Eynard, Federico Monti, and Michael Bronstein. 2020. Temporal Graph Networks for Deep Learning on Dynamic Graphs. In *ICML 2020 Workshop on Graph Representation Learning.*

[32] Ryan Rossi and Nesreen Ahmed. 2015. The network data repository with interactive graph analytics and visualization. In *Twenty-ninth AAAI conference on artificial intelligence.*

[33] Frederic Sala, Chris De Sa, Albert Gu, and Christopher Ré. 2018. Representation tradeoffs for hyperbolic embeddings. In *International conference on machine learning.* PMLR, 4460–4469.

[34] Aravind Sankar, Yanhong Wu, Liang Gou, Wei Zhang, and Hao Yang. 2020. Dysat: Deep neural representation learning on dynamic graphs via self-attention networks. In *Proceedings of the 13th international conference on web search and data mining.* 519–527.

[35] Ramit Sawhney, Shivam Agarwal, Arnav Wadhwa, and Rajiv Shah. 2021. Exploring the scale-free nature of stock markets: Hyperbolic graph learning for algorithmic trading. In *Proceedings of the Web Conference 2021.* 11–22.

[36] Youngjoo Seo, Michaël Defferrard, Pierre Vandergheynst, and Xavier Bresson. 2018. Structured sequence modeling with graph convolutional recurrent networks. In *International conference on neural information processing.* Springer, 362–373.

[37] Jianing Sun, Zhaoyue Cheng, Saba Zuberi, Felipe Pérez, and Maksims Volkovs. 2021. Hgcf: Hyperbolic graph convolution networks for collaborative filtering. In *Proceedings of the Web Conference 2021.* 593–601.

[38] Li Sun, Zhongbao Zhang, Jiawei Zhang, Feiyang Wang, Hao Peng, Sen Su, and S Yu Philip. 2021. Hyperbolic variational graph neural network for modeling dynamic graphs. In *Proceedings of the AAAI Conference on Artificial Intelligence*, Vol. 35. 4375–4383.

[39] Shang-Hua Teng et al. 2016. Scalable algorithms for data and network analysis. *Foundations and Trends® in Theoretical Computer Science* 12, 1–2 (2016), 1–274.

[40] Rakshit Trivedi, Mehrdad Farajtabar, Prasenjeet Biswal, and Hongyuan Zha. 2019. Dyrep: Learning representations over dynamic graphs. In *International conference on learning representations.*

[41] Aäron van den Oord, Sander Dieleman, Heiga Zen, Karen Simonyan, Oriol Vinyals, Alex Graves, Nal Kalchbrenner, Andrew W. Senior, and Koray Kavukcuoglu. 2016. WaveNet: A Generative Model for Raw Audio. In *The 9th ISCA Speech Synthesis Workshop, Sunnyvale, CA, USA, 13-15 September 2016.* ISCA, 125.

[42] Ashish Vaswani, Noam Shazeer, Niki Parmar, Jakob Uszkoreit, Llion Jones, Aidan N Gomez, Łukasz Kaiser, and Illia Polosukhin. 2017. Attention is all you need. *Advances in neural information processing systems* 30 (2017).

[43] Petar Veličković, Guillem Cucurull, Arantxa Casanova, Adriana Romero, Pietro Liò, and Yoshua Bengio. 2018. Graph Attention Networks. In *International Conference on Learning Representations.*

[44] Xiao Wang, Yiding Zhang, and Chuan Shi. 2019. Hyperbolic heterogeneous information network embedding. In *Proceedings of the AAAI conference on artificial intelligence*, Vol. 33. 5337–5344.

[45] Yiwei Wang, Yujun Cai, Yuxuan Liang, Henghui Ding, Changhu Wang, and Bryan Hooi. 2021. Time-Aware Neighbor Sampling for Temporal Graph Networks. *arXiv preprint arXiv:2112.09845* (2021).

[46] Max Welling and Thomas N Kipf. 2016. Semi-supervised classification with graph convolutional networks. In *J. International Conference on Learning Representations (ICLR 2017).*

[47] Xian Wu, Baoxu Shi, Yuxiao Dong, Chao Huang, and Nitesh V Chawla. 2019. Neural tensor factorization for temporal interaction learning. In *Proceedings of the Twelfth ACM international conference on web search and data mining.* 537–545.

[48] Z Wu, S Pan, G Long, J Jiang, and C Zhang. 2019. Graph WaveNet for Deep Spatial-Temporal Graph Modeling. In *The 28th International Joint Conference on Artificial Intelligence (IJCAI).* International Joint Conferences on Artificial Intelligence Organization.

[49] Cheng Yang, Chunchen Wang, Yuanfu Lu, Xumeng Gong, Chuan Shi, Wei Wang, and Xu Zhang. 2022. Few-shot Link Prediction in Dynamic Networks. In *Proceedings of the Fifteenth ACM International Conference on Web Search and Data Mining.* 1245–1255.

[50] Carl Yang, Jieyu Zhang, Haonan Wang, Sha Li, Myungwan Kim, Matt Walker, Yiou Xiao, and Jiawei Han. 2020. Relation learning on social networks with

multi-modal graph edge variational autoencoders. In *Proceedings of the 13th International Conference on Web Search and Data Mining*. 699–707.

[51] Menglin Yang, Zhihao Li, Min Zhou, Jiahong Liu, and Irwin King. 2022. HICF: Hyperbolic Informative Collaborative Filtering. In *Proceedings of the 28th ACM SIGKDD Conference on Knowledge Discovery and Data Mining*. 2212–2221.

[52] Menglin Yang, Min Zhou, Marcus Kalander, Zengfeng Huang, and Irwin King. 2021. Discrete-time temporal network embedding via implicit hierarchical learning in hyperbolic space. In *Proceedings of the 27th ACM SIGKDD Conference on Knowledge Discovery & Data Mining*. 1975–1985.

[53] Menglin Yang, Min Zhou, Jiahong Liu, Defu Lian, and Irwin King. 2022. HRCF: Enhancing collaborative filtering via hyperbolic geometric regularization. In *Proceedings of the ACM Web Conference 2022*. 2462–2471.

[54] Aya Zaki, Mahmoud Attia, Doaa Hegazy, and Safaa Amin. 2016. Comprehensive survey on dynamic graph models. *International Journal of Advanced Computer Science and Applications* 7, 2 (2016).

[55] Sixiao Zhang, Hongxu Chen, Xiao Ming, Lizhen Cui, Hongzhi Yin, and Guandong Xu. 2021. Where are we in embedding spaces?. In *Proceedings of the 27th ACM SIGKDD Conference on Knowledge Discovery & Data Mining*. 2223–2231.

[56] Yiding Zhang, Xiao Wang, Chuan Shi, Xunqiang Jiang, and Yanfang Fanny Ye. 2021. Hyperbolic graph attention network. *IEEE Transactions on Big Data* (2021).

[57] Yiding Zhang, Xiao Wang, Chuan Shi, Nian Liu, and Guojie Song. 2021. Lorentzian graph convolutional networks. In *Proceedings of the Web Conference 2021*. 1249–1261.

[58] Ling Zhao, Yujiao Song, Chao Zhang, Yu Liu, Pu Wang, Tao Lin, Min Deng, and Haifeng Li. 2019. T-gcn: A temporal graph convolutional network for traffic prediction. *IEEE Transactions on Intelligent Transportation Systems* 21, 9 (2019), 3848–3858.

[59] Lekui Zhou, Yang Yang, Xiang Ren, Fei Wu, and Yueting Zhuang. 2018. Dynamic network embedding by modeling triadic closure process. In *Proceedings of the AAAI conference on artificial intelligence*, Vol. 32.

[60] Yuan Zuo, Guannan Liu, Hao Lin, Jia Guo, Xiaoqian Hu, and Junjie Wu. 2018. Embedding temporal network via neighborhood formation. In *Proceedings of the 24th ACM SIGKDD international conference on knowledge discovery & data mining*. 2857–2866.

A APPENDIX

A.1 Notations

Part of notations in our paper are summarized in Table 5.

Table 5: Notations.

Symbols	Descriptions
$\mathcal{G}$	Discrete dynamic graph represented by snapshots.
$\mathcal{G}_t$	Snapshot of $\mathcal{G}$ at timestamp t.
$\mathbb{H}_c^n$	n-dimensional hyperbolic manifold with curvature $-c$.
$g^{c,\mathbb{H}}$	Riemannian metric corresponding to the manifold $\mathbb{H}$.
$\mathcal{T}_\mathbf{x}\mathbb{H}_c^n$	Tangent space of $\mathbb{H}_c^n$ at point $\mathbf{x}$.
$\mathbb{B}_c^n$	Poincaré ball manifold corresponding to $\mathbb{H}_c^n$.
d	Dimension of node representations.
K	Truncated diffusion steps in HDGC.
L	Layer number of HDGC.
S	Convolution kernel size of HDCC.
D	Dilated depth of HDCC.
D'	Layer number of gated HDCC module.
$\mathbf{A}$	Bi-direct adjacent matrix of a static graph or snapshot.
$\mathbf{X}_{t,k}^l$	k-th step of HDGC at layer l, timestamp t.
$\mathbf{H}_t$	Temporal information earlier than timestamp t.
$\mathbf{F}$	Kernel metrix of HDCC.
$\mathbf{Z}_t$	Node representations at timestamp t.
$\mathcal{L}_{\text{HTC}}^t$	Hyperbolic temporal consistency at timestamp t.
$\mathcal{L}_{\text{CE}}^t$	Cross-entropy like loss at timestamp t.
$\mathbf{W}, \mathbf{b}$	Trainable parameters.

A.2 Experimental Details

For all baselines, we take the recommended parameter settings unless otherwise noted. For our proposed HGWaveNet, the parameters are set as follows: the truncated diffusion step $K = 2$, the layer number of HDGC $L = 2$, the dilation depth for HDCC $D = 3$, kernel

size $S = 2$, the layer number for gated HDCC is valued as 4, and the hyper-parameters r, s in Fermi-Dirac decoder are taken to be 2 and 1 separately. All involved curvatures are initialized as 1 and keep trainable during the training process. For fairness, the representation dimension is set to 16 for all methods. All experiments are run on a machine with 2 × Intel Xeon Gold 6226R 16C 2.90 GHz CPUs, 4 × GeForce RTX 3090 GPUs.

A.3 Supplementary Experiments

In Table 6, 7 and 8, we give out the supplementary experimental results for parameter analysis in Section 5.4. All these experiments are evaluated by AUC score on temporal link prediction task.

Table 6: The influence of representation dimension.

Dimension	Enron	DBLP	AS733	FB	HepPh	MovieLens
16	96.86	89.96	98.78	89.51	92.37	91.90
8	96.56	89.49	98.67	88.74	90.20	88.44
4	96.64	89.24	98.36	88.51	88.76	87.90
2	96.41	88.84	97.95	87.87	88.42	86.55

Table 7: The influence of truncated diffusion step K.

K	Enron	DBLP	AS733	FB	HepPh	MovieLens
1	94.95	89.51	97.97	85.99	90.61	84.35
2	96.86	89.96	98.78	89.51	92.37	91.90
3	96.88	89.62	98.95	90.28	92.72	92.36
4	96.86	89.67	98.94	90.39	92.81	92.42

Table 8: The influence of dilated depth D.

D	Enron	DBLP	AS733	FB	HepPh	MovieLens
1	91.14	88.67	94.98	73.69	87.38	80.44
2	92.16	89.89	97.12	83.18	90.41	87.52
3	96.86	89.96	98.78	89.51	92.37	91.90
4	97.17	89.62	98.93	89.99	93.17	91.47